RSC Advances

ROYAL SOCIETY OF CHEMISTRY

www.rsc.org/advances

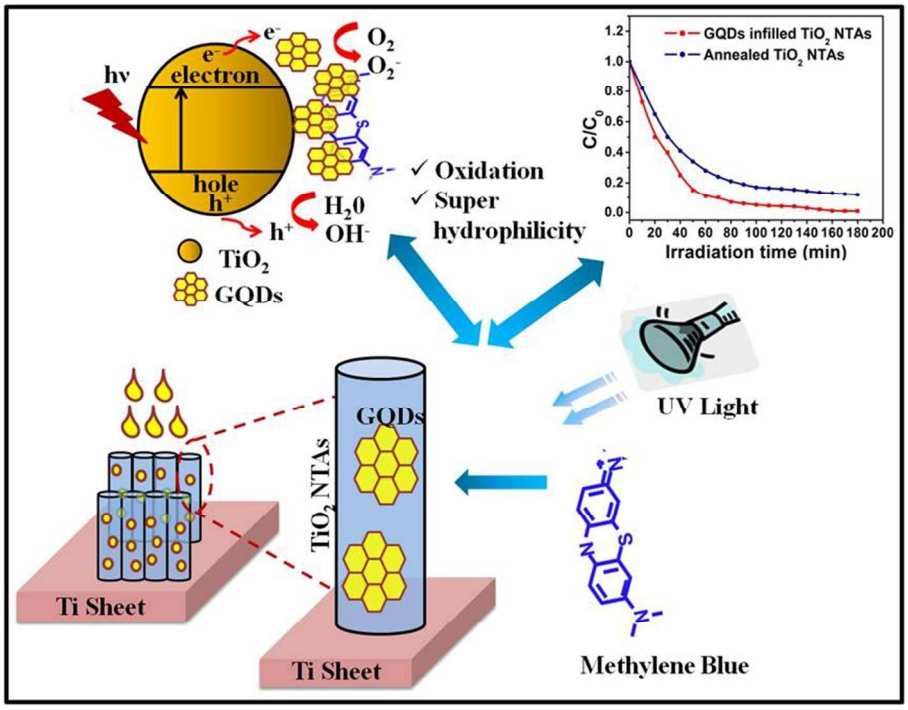

A novel strategy has been proposed to fabricate graphene quantum dots infilled TiO2 nanotubes arrays for high- performance photocatalyst application.
254x190mm (96 x 96 DPI)

RSC Advances

Cite this: DOI: 10.1039/c0xx00000x

www.rsc.org/xxxxxx

ARTICLE TYPE

A novel strategy to enhance ultraviolet light driven photocatalysis from graphene quantum dots infilled TiO_2 nanotubes arrays

Bipin Kumar Gupta[a],*, Garima Kedawat[b], Yogyata Agrawal[a], Pawan Kumar[a], Jaya Dwivedi[a] and S. K. Dhawan[a]

Received (in XXX, XXX) XthXXXXXXXXX 20XX, Accepted Xth XXXXXXXXX 20XX
DOI: 10.1039/b000000x

Herein, a novel strategy has been proposed to fabricate graphene quantum dots (GQDs) infilled titanium dioxide (TiO_2) nanotube arrays (NTAs) structure for methylene blue (MB) dye degradation activity under UV light (365 nm) irradiation. GQDs are infilled inside the TiO_2 NTAs (via anodic oxidation of Ti sheet) through an impregnation method. Moreover, the morphology of TiO_2 NTAs is well maintained after filling the GQDs inside, which is favorable for mass transfer. The peak intensity of photoluminescence (PL) spectra of GQDs infilled TiO_2 NTAs catalyst is lower than that of annealed TiO_2 NTAs and a strong violet UV emission is obtained at 387 nm upon 252 nm deep UV excitation wavelength. The photocatalytic activities of TiO_2 NTAs are evaluated in terms of the efficiencies of photo-decomposition and adsorption of MB in aqueous solution under UV light irradiation, after the impregnation of GQDs inside the TiO_2 NTAs. The highly-efficient photocatalytic activity is attributed to broad absorption in the visible wavelength region, large photo-induced charge separation through transfer of photo-generated electrons from TiO_2 NTAs to GQDs, as well as, the strong adsorption capacity of GQDs to MB molecules. Thus, the GQDs infilled TiO_2 NTAs could be widely used as a photocatalyst for treating the organic contaminant in the field of environmental protection.

1. Introduction

Photocatalysts, which accelerates chemical reactions upon light irradiation, have been paid a great attention in environmental remediation and solar fuels production due to its fascinating properties such as quantum confinement and enhanced reactivity.[1-3] Photocatalyst has a high potential for a wide range of industrial applications including mineralization of organic pollutant, purification of disinfects in water and air, production of renewable fuels and organic synthesis.[1,3] The degradation of organic dyes using the semiconductor photocatalyst materials is a promising resolution for wastewater purification.[4,5]

Titanium dioxide (TiO_2) with low cost, non-toxicity, high redox-ability and chemical stability, has been extensively studied as a most attractive photocatalyst semiconductor for energy saving and environmental protection due to its intriguing optical and electric properties.[6-8] However, due to its wide band gap of ~ 3.2 eV, it can be excited only by the ultraviolet radiation that occupies about 4% of the solar light, confines its applications in various fields.[9,10] Moreover, it also exhibits poor visible light absorption, low efficiency in light utilization and high recombination rate of photo-generated electron/hole pairs in comparison to the time of chemical interaction of TiO_2 with the adsorbed contaminants, which greatly retard its photocatalytic performance.[11,12] In order to utilize the solar energy radiation, the development of catalyst materials which reduce the recombination charge carrier time and harvest more photons in the visible light region of the solar spectrum, has become an active research area in recent years. Thus, the substantial efforts have been adopted to modify the TiO_2 structures and properties such as the charge separation efficiency and enhance photoactivity in visible range.[9,13]

In particular, vertically aligned photocatalyst TiO_2 three-dimensional (3D) nanotube arrays (NTAs) have been engrossing attention to improve the photocatalytic activity because of their high orientation, tunable mesopore size, high internal surface area, convenient recycling and ion-changeable ability between interfaces.[5,14,15] In addition to this, the TiO_2 photocatalyst has also been extensively studied with the novel heterostructure functional materials such as narrow band-gap semiconductors, metal and non-metal elements and dye molecules to increase the efficiency and range of photon absorption.[16-18] Carbon based materials as graphene oxide, graphene sheets and graphene quantum dots anchor with the TiO_2 photocatalyst are highlighted as a cost-effective UV driven photocatalyst in the visible region with

enhanced activity due to the retarded charge recombination, increased reaction sites and expanded light absorption range properties.[19,20] These nanostructures concentrate the organics near the photocatalyst surface which could facilitate effective photo-degradation of pollutants under visible light.

Graphene quantum dots (GQDs) have a perfect sp^2-hybridized two-dimensional (2D) honeycomb carbon structure with better electron-transport, electron-accepting and stable photo luminescence properties.[21,22] These have emerged and ignited tremendous research interest due to the pronounced quantum confinement and edge effects. In particular, owing to its zero band gap, large surface area and high electron mobility, it also provides a direct path to charge-transport of photo generated charge carriers, which increases the lifetime of electron-hole pairs, arises through the incident of light irradiation on TiO_2 NTAs.[21,22] Thus, their photocatalyst performances for the environmental remediation and energy conversion applications become greatly enhanced. However, to the best of our knowledge, there are few reports on heterojunction between GQDs and TiO_2 nanotubes for photocatalytic applications. [16, 19, 22-24] Herein, we demonstrated a novel method to fabricate an efficient GQDs infilled TiO_2 NTAs photocatalysts. The highly orientated TiO_2 3D NTAs and GQDs have been fabricated using anodic oxidation of Ti sheet and facile chemical synthesis method, respectively. GQDs are drop casted for impregnated into the inter-tubular voids of vertically aligned annealed TiO_2 3D NTAs. Microstructure (XRD, Raman and XPS) analysis confirmed the formation of TiO_2 anatase phase, GQDs and covalent bonds occurred between Ti and C atoms through the filling of GQDs into the TiO_2 NTAs. Their photocatalyst activity has been determined by degradation of methylene blue (MB) as an organic pollutant molecule under UV light (365 nm) irradiation. It has displayed a strong optical response under visible-light range, efficient separation of photogenerated electron–hole pairs, as well as high adsorption capacity for MB. Moreover, the photocatalytic activity, stability and reusability of novel GQDs/TiO_2 3D NTAs hybrid structure are substantially enhanced as compared to the pristine GQDs and TiO_2 NTAs. The structure and interfacial electronic interaction between TiO_2 and GQDs have also systematically investigated.

2. Experimental

2.1 Materials

The titanium (Ti) sheet (99.8% purity, size ~0.5 mm×~20 mm×~15 mm) and carbon fibers were purchased from Sigma-Aldrich and Fibre Glast Development Corporation, respectively. Methylene blue (MB) was obtained commercially from Aldrich Chemical Co. Ammonium fluoride (NH_4F), ethylene glycol ($C_2H_6O_2$), sodium carbonate (Na_2CO_3) and all other reagents were of analytical (AR) grade and used as received without further purification. Double distilled water was used throughout the experiments.

2.2 Synthesis of vertically aligned TiO_2 3D NTAs

Vertical aligned TiO_2 3D NTAs were fabricated by anodic oxidation of 0.5 mm thick Ti sheet. Prior to anodization, Ti sheet was ultrasonically cleaned in acetone and ethanol, respectively. The schematic representation of experimental setup is shown in Fig. 1. The electrochemical anodization of Ti sheet was carried out using two-electrode configuration with Ti sheet as the test electrode and platinum sheet as counter electrode. Both the electrodes were immersed in electrolytic solution which contained in a beaker with keeping them a distance of 2 cm and Cu-wires were used for the connection through the parallel electrodes. The cleaned Ti sheet was anodized at 40 V for 4 hours (condition optimized experimentally) in electrolyte solution which is composed of 0.3 wt% NH_4F and 5.0 vol% deionized water in an ethylene glycol solution. The obtained amorphous NTAs samples were annealed at 500°C for 2 hours to acquire pure anatase phase of vertically aligned TiO_2 3D NTAs. The surface morphology of annealed samples was analyzed by scanning electron microscope, which revealed that after anodization and annealing process, the large outer diameter of tube was ~ 110 nm with length 2000 nm.

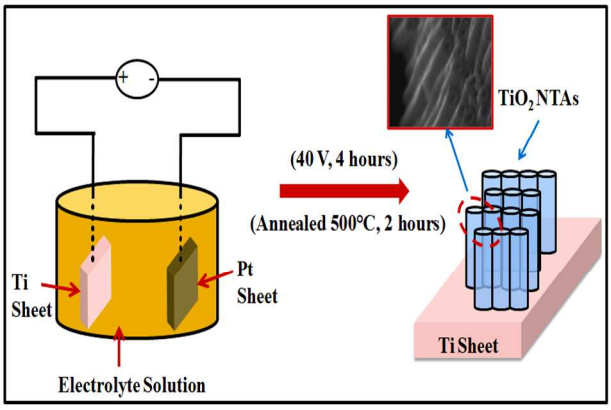

Fig. 1. Schematic representation of experimental set-up of electrochemical anodization process to obtain TiO_2 3D NTAs on Ti sheet.

2.3 Synthesis of graphene quantum dots

Carbon fibers (0.30 g) were added into a mixture 3:1 of concentrated H_2SO_4 (60 mL) and HNO_3 (20 mL). The solution was ultrasonicated (frequency; 25 kHz) for 2 hours and stirred for 24 hours at different temperatures of 80^0C, 100^0C and 120^0C, respectively. Then, mixture was cooled and diluted with deionized (DI) water (800 mL) and adjusted the pH about 8 using Na_2CO_3. The final solution was further dialyzed in a dialysis bag (retained molecular weight: 2000 Da) for 3 days and thus, graphene quantum dots (GQDs) were obtained.[25] Furthermore, to characterize the GQDs, the film of GQDs was deposited on the quartz plate.

2.4 Synthesis of graphene quantum dots infilled TiO_2 3D NTAs

The as synthesized GQDs were ultrasonically dispersed into ethanol solution via ultrasonication at frequency 25 kHz for 1 hour to form a homogeneous suspension with a concentration of 0.05 mg/mL. The resultant solution was drop casted on mouth surface of the highly oriented TiO_2 3D NTAs (40 V, 4 hours, 500°C) using micro-syringe, as shown in Fig. 2. It is highly-efficient technique to fill the GQDs into the TiO_2 nanotubes, owing to its hydrophilic nature. Prior to infilled GQDs in TiO_2 nanotubes, the hydrophilic nature of annealed TiO_2 3D NTAs was examined using contact angle measurement. It can be found in the Fig. S1 (see supporting information). The contact angle between TiO_2 3D nanotubes and water droplet is about 0° and water is easily spread out on TiO_2 nanotubes surface which enables quantum dot to make easy entry into TiO_2 NTAs. Thus, this process provides efficient entry of GQDs through the hollow mouth of TiO_2 nanotubes within few seconds. The contact angle experiment is evidenced that the water based GQDs are possible to fill efficiently into the TiO_2 NTAs which can be clearly seen in Fig. 2. Several statistical runs have been performed to optimize the amount of drop, size and speed of drop cast to avoid any kind of collapse of TiO_2 nanotubes. After drop cast process, once infilling phenomenon is finished, the sample of nanotubes arrays was slowly washed with water in multiple times to remove any kind of stick quantum dots on outer wall of TiO_2 nanotubes. The infilled GQDs build chemical complexation within the internal walls of TiO_2 nanotubes, which doesn't come out and even doesn't desorbed when GQDs infilled in TiO_2 nanotubes arrays kept into aqueous solution or dispersed in aqueous solution as well as in any medium. The GQDs have played a significant role to obtain the enhanced photocatalyst activity of TiO_2 NTAs.

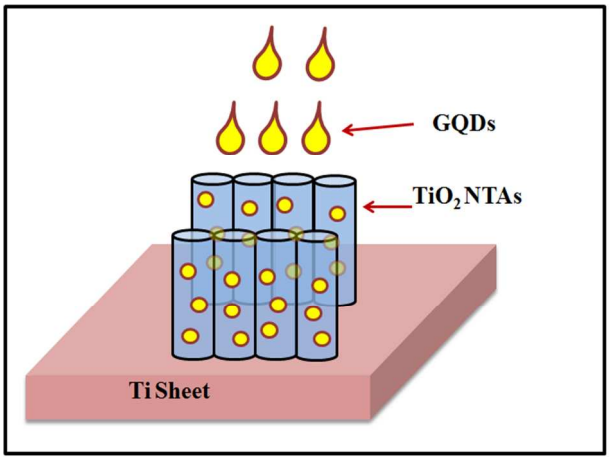

Fig. 2: The systematic process of GQDs infilled TiO_2 NTAs.

2.5 Characterizations

The crystalline properties of catalysts were evaluated by x-ray diffraction (XRD) measurements with a Rigaku Mini-flex Diffractometer using Cu-Kα_1 radiation with a Ni filter (λ = 1.5406 Å at 30 kV and 15 mA). Prior to XRD measurement, the diffractometer was calibrated with silicon powder (d_{111}=3.1353 Å).[26] Raman spectra were obtained using Renishaw InVia Raman spectrometer, UK with an excitation source of 514.5 nm. The XPS analysis was performed in an ultra-high vacuum (UHV) chamber equipped with a hemispherical electron energy analyzer (Perkin Elmer, PHI1257) using non-monochromatized Al Kα source (excitation energy of 1486.7 eV) with a base pressure of 4 x10^{-10} torr at room temperature. The surface morphology, length and diameter of TiO_2 NTAs were calculated by field emission scanning electron microscopy (FESEM, Model No. EVO-MA 10 VPSEM). The microstructural studies were performed using high-resolution transmission electron microscopy (HRTEM, Model No. Technai G20-twin, 200 kv with super twin lenses having point and line resolution of 0.144 nm and 0.232 nm, respectively) equipped with energy dispersive x-ray analysis (EDAX) facilities. The photoluminescence (PL) spectra were obtained using luminescence spectrometer (Edinburgh, FLSP − 920) with EPL 375 nm picosecond pulsed diode laser as a source of excitation.

2.6 Photocatalytic degradation of MB

The relative photocatalytic activities of GQDs infilled TiO_2 NTAs were evaluated by spectrophotometrically with an ATI Unicam UV spectrometer by using a 1cm quartz cuvette with a resolution of 2 nm. Prior to exposure to UV lights, GQDs infilled TiO_2 NTAs composite as photocatalyst was immersed into the MB solution (concentration 20 µM in water) for at least 45 min in the dark in a nitrogen atmosphere until no further decrease of the absorption intensity of MB was observed. The optical absorption profiles were acquired at different exposure times to the UV lights (365 nm, 6 W). Note, the solution was blanketed with a nitrogen atmosphere during the entire experimental procedure.

3. Results and discussion

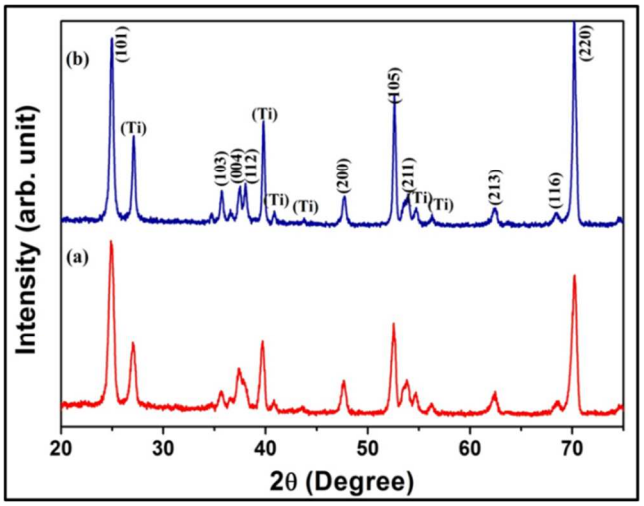

Fig. 3: The XRD patterns of (a) annealed TiO_2 3D NTAs and (b) GQDs infilled TiO_2 3D NTAs.

The gross structures and phase analysis of as-prepared samples were analyzed by XRD. Fig. 3 presents the XRD patterns of annealed TiO_2 3D NTAs (Fig. 3a) and GQDs infilled TiO_2 3D NTAs (Fig. 3b). Quantitative analysis of Fig. 3a shows that all of the diffraction peaks are ascribed to TiO_2 and Ti substrate. The typical diffraction peak (101) centred at 25.1° indicates the TiO_2 anatase phase (JCPDS No. 21-1272), which is formed after annealing at 500°C for 2 hours. The peaks correspond to the (101), (103), (004), (112), (200), (105), (211), (213), (116) and (220) plane of anatase phase with tetragonal crystal structure with space group S.G. $I4_1/amd$ (141). The lattice parameters were calculated by standard unit cell software with the help of obtained d-values and respective hkl planes, a = (3.79632±0.0091) Å, c = (9.5832±0.0097) Å for annealed TiO_2 NTAs samples. Anatase TiO_2 exhibits a better performance due to the higher Fermi level and the lower recombination rate of its photo-generated electrons and holes than those of the rutile phase.[17] The average crystalline size for annealed TiO_2 3D NTAs samples is 121 nm with respect to (101) plane, which is estimated using Scherer's equation. It is noticed in Fig. 3b that the diffraction patterns from carbon species is not observed, which may result from the small amount and weak intensity of GQDs and the main peak of graphene (2θ = 24°) may have been shielded by the main peak of anatase TiO_2 at (2θ = 25.1°).[20] There is no change in phase of TiO_2 NTAs, as in sample annealed TiO_2 NTAs (Fig. 3a) and GQDs infilled annealed TiO_2 3D NTAs (Fig. 3b). These features indicate that the crystalline structure of TiO_2 NTAs is not influenced by the filling of GQDs into TiO_2 3D NTAs. The XRD pattern of GQDs is determined in Fig. S2a (see supporting information). The broad diffraction peak centered at 2θ = 24.4° is attributed to the (002) plane of the carbon structure with hexagonal phase (JCPDS No. 75-1621). The broad peak signifies the low crystallinity and small size of GQDs, which has been verified with the TEM measurements.

Raman spectroscopy was employed to confirm the formation of a TiO_2 anatase phase and the existence of GQDs into the inner walls of TiO_2 NTAs. The Raman spectra of annealed TiO_2 3D NTAs and GQDs infilled TiO_2 3D NTAs is shown in Fig. 4(a,b), respectively. The Raman characteristic peaks for both the sample at around 394, 516 and 642 cm^{-1} are obtained, which corresponds to the B_{1g}, $A_{1g} + B_{1g}$ and E_g modes of vibration of anatase phase of TiO_2, respectively.[27] The observations are consistent with the XRD results. Two additional peaks at about 1354 and 1600 cm^{-1} for the graphene structure are also observed in the Raman spectrum of GQDs infilled TiO_2 3D NTAs (Fig. 4b), which can be assigned to disordered sp^2 carbon (D-band) and well-ordered graphite (G-band), respectively.[25] The intensity ratio of D to G band (I_D/I_G = 0.846) indicates the disorder in the graphene which originates from defects associated with grain boundaries, vacancies and amorphous carbons. The Raman spectrum of GQDs is shown in Fig. S2b (see supporting information). This confirms a significant growth and incorporation of carbon on the internal surfaces of TiO_2 nanotubes. The electronic interactions between the graphene and

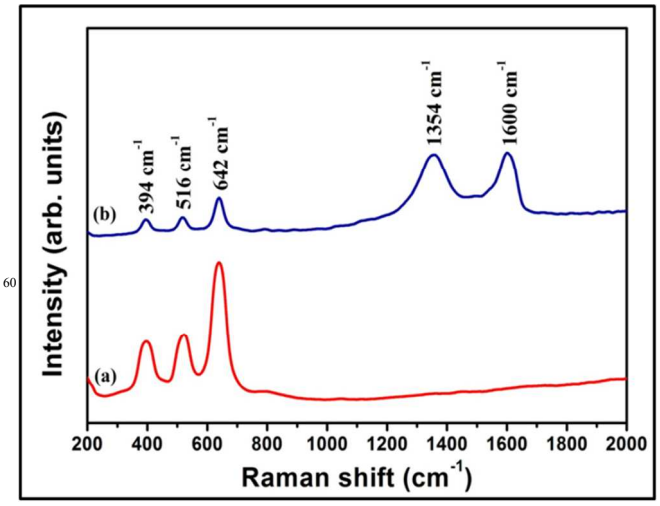

Fig. 4: The Raman spectra of (a) annealed TiO_2 3D NTAs and (b) GQDs infilled TiO_2 3D NTAs.

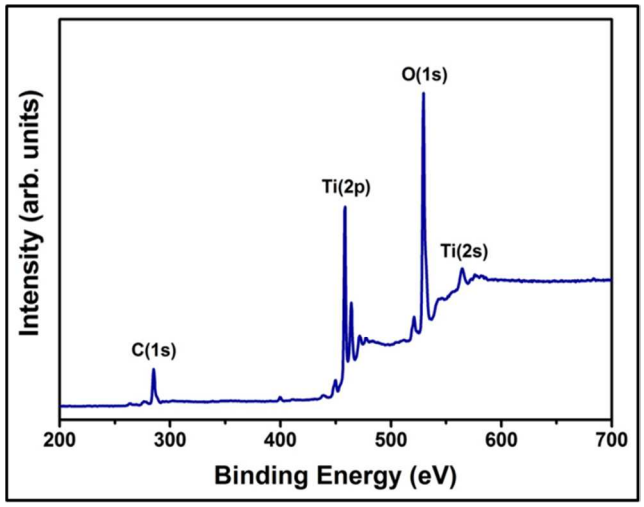

Fig. 5: XPS spectra of GQDs infilled TiO_2 3D NTAs.

TiO_2 components in the GQDs infilled TiO_2 3D NTAs were revealed by XPS measurements.

The GQDs infilled TiO_2 3D NTAs were employed for XPS analysis to detect the purity, bonding states and chemical composition of TiO_2 nanotube and GQDs, the XPS spectrum is shown in Fig. 5. It is direct evidence of the TiO_2 band structure through the filling of GQDs. All the peak signals are endorsed to only titanium, oxygen and carbon elements which show the high purity of synthesized GQDs infilled TiO_2 3D NTAs. According to XPS spectrum, the characteristic deconvolution peaks of C1s, O1s and Ti(2p) core levels of GQDs infilled TiO_2 3D NTAs are given in Fig. S3 (see supporting information). The graphene peak (Fig. S3a) is assigned with binding energy of C1s electrons of sp_2 hybridized carbon at around 291 eV. The $Ti2p_{1/2}$ and $Ti2p_{3/2}$ electrons are attributed at 463.9 eV and 458.24eV binding energy for the titanium (Fig. S3b), respectively and O1s electron is obtained at 529.5 eV binding energy for the Oxygen (Fig. S3c) in GQDs infilled TiO_2 3D NTAs structure. The characteristic deconvolution peaks (filled area) of GQDs is given in Fig. S3a.

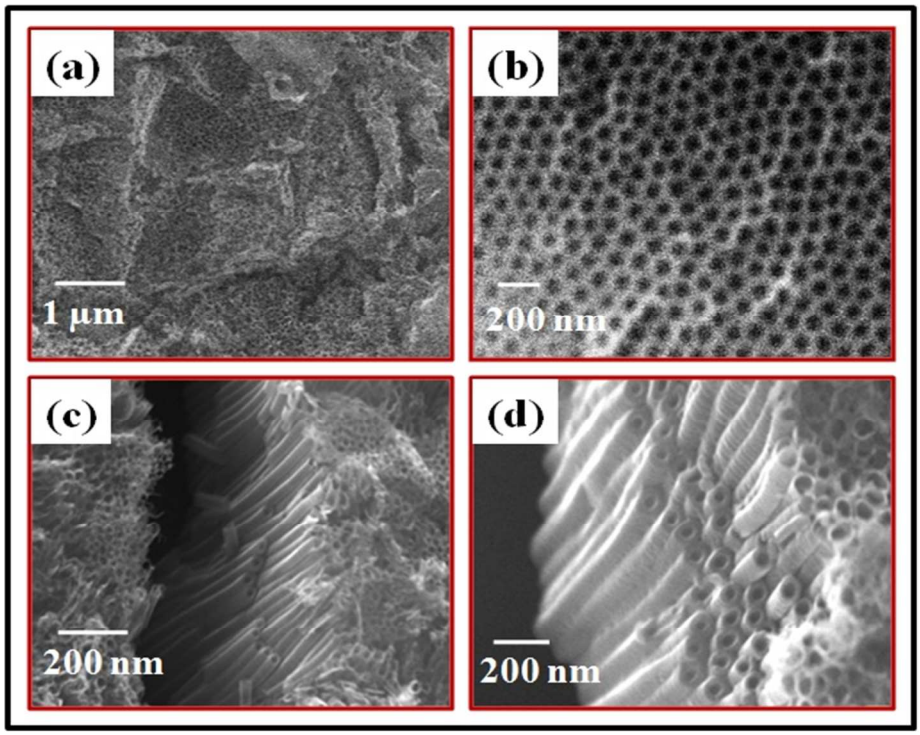

Fig. 6: SEM images; (a) Top view, (b) magnified view of (a), (c) lateral view and (d) magnified view of (c) of annealed TiO_2 3D NTAs.

The typical XPS peaks at 292.2, 293.1, and 295.2 eV are appeared which can assign to the presence of the C–C, C–O, and C=O functional groups. This intimate the electronic interactions between the carbon and TiO_2 nanotube in GQDs infilled TiO_2 3D NTAs for the unique interfacial charge transfer upon photo-irradiation process. For morphological analysis, scanning electron microscope (SEM) and transmission electron microscope (TEM) were used to characterize the GQDs infilled TiO_2 3D NTAs structure. Fig. 6 (a-d) represents the top and lateral view of SEM images of high density, vertically aligned, annealed TiO_2 3D NTAs formed on Ti substrate with an average outer diameter of ~110 nm and maximum length ~2000 nm. The alignment of sample does not get disturb after annealing and consist of uniform open nanotubes of TiO_2 with good crystallinity.

To obtain morphology, crystallite size and composition of TiO_2 3D NTAs and GQDs infilled TiO_2 3D NTAs, the TEM images and EDX spectrum are analyzed in Fig. 7. The TEM image of isolated annealed TiO_2 nanotube with outer diameter ~ 110 nm is depicted in Fig. 7a and inset shows the HRTEM image of TiO_2 3D NTAs with high quality lattice fringes without distortion. It clearly demonstrates the crystal quality of TiO_2 nanotubes, which is consistent with the XRD results. The precise observation of HRTEM image indicates that the estimated interplaner spacing of adjacent lattice fringes, as highlighted by black lines, is estimated to be ~0.35 nm which corresponds to the (101) plane of TiO_2 anatase phase. The TEM image of GQDs is shown in Fig. 7b. The GQDs are found to exhibit a narrow size distribution with an average crystallite size of ~8-12 nm. The HRTEM image of GQDs with ~0.40 nm interplaner spacing of adjoining lattice fringes corresponding to the (002) plane of GQDs is shown in inset of Fig. 7b. The TEM image of GQDs infilled TiO_2 3D NTAs is given in Fig. 7c, where yellow circle represents the GQD particle. The graphene is well established in binding to the TiO_2 nanotube through the covalent bonding or complexation without aggregation effects. The strong interaction between GQDs and TiO_2 would allow the transfer of electrons from TiO_2 to GQDs during the photo irradiation process which could significantly increase the separation of photo-induced charges and leads to improve the photocatalytic activity performance in the degradation of organic pollutants. Furthermore, the evidence of quality as well as elemental composition of TiO_2 nanotubes and GQDs was evaluated by EDAX analysis. The spot EDAX measurement was performed with reduced beam spot size and low accelerating potential to enhance signal to noise ratio. The EDAX mapping images of GQDs infilled TiO_2 3D NTAs is also shown in Fig. 7d. The EDAX analysis indicates the presence of titanium, oxygen, fluorine, and carbon elements in GQDs infilled TiO_2 3D NTAs composite structure. The carbon content is present in relatively lower intensity as compared to the higher intensity of titanium and oxygen content. The presence of fluorine element is due to the electrolyte solution. Further, the typical HRTEM image was taken to evidence the interface between the GQDs and TiO_2, as shown in inset of Fig. 7d. The yellow mark line clearly reveals the separate lattice of the GQDs and TiO_2 with estimated their d-spacing. The GQDs are well established in binding to TiO_2 nanotubes through covalent bonding or complexation without aggregation effects.

Photoluminescence (PL) is an essential direct optical probe to investigate the efficiency of charge carrier trapping and

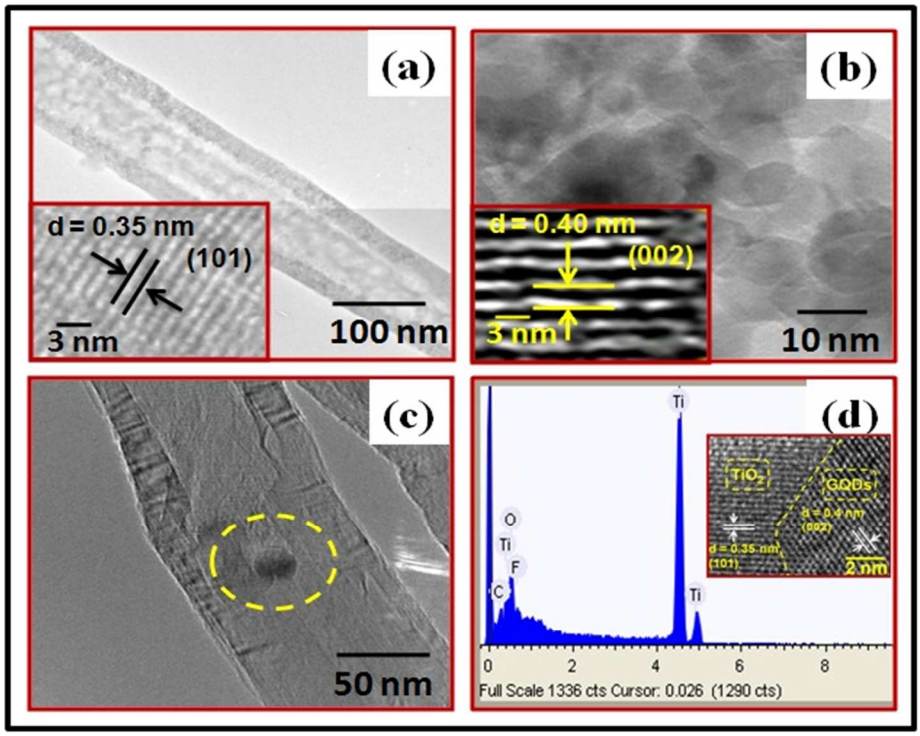

Fig. 7: (a) TEM image of isolated annealed TiO_2 nanotube; inset shows the HRTEM image of (a), (b) TEM image of GQDs; inset shows the HRTEM image of (b), (c) TEM image of GQDs infilled isolated TiO_2 nanotube; yellow circle represents the GQD particle and (d) EDAX mapping spectrum of GQDs infilled TiO_2 3D NTAs; inset shows the HRTEM image of GQDs infilled TiO_2 NTAs where yellow mark line clearly reveals the separate lattice of the GQDs and TiO_2.

understand the rate of e^-/h^+ pairs in semiconductor particles. The PL emission spectra of annealed TiO_2 NTAs and GQDs infilled TiO_2 3D NTAs at 252 nm excitation wavelength is exhibited in Fig. 8 and inset shows the CIE (chromaticity diagram) color coordinates of annealed TiO_2 3D NTAs which is obtained from emission spectra of annealed TiO_2 nanotube using chromaticity diagram, x = 0.2243 and y = 0.1808. The optical image of sample chamber of PL spectrometer is given in Fig. S4 (see supporting information), where annealed TiO_2 3D NTAs on Ti sheet were loaded. The annealed TiO_2 3D NTAs sample is shown in Fig. S4a. The annealed TiO_2 3D NTAs sample has been placed in spectrometer chamber to optimize the position of TiO_2 3D NTAs. The sample exhibits strong violet UV emission under deep UV light at 252 nm excitation wavelength which is shown in Fig. S4b. The strong ultraviolet emission near visible region 387 nm (~3.2 eV) is observed, as shown in Fig. 8; the excitation wavelength is 252 nm. The PL results reveal that the intensity of annealed TiO_2 is higher than the GQDs infilled TiO_2 3D NTAs which were expected because the annealing at 500°C higher temperature is introduced more defects and oxygen vacancy in the TiO_2 NTAs and strong PL occurs. The reduction of PL emission intensity suggests that GQDs in the hybrid structure can restrain the recombination of electron and holes and promotes the separation of electron–hole pairs and extend the life of electrons. The PL spectra peaking at 387 nm (~3.2 eV) corresponds to the direct recombination between electrons in the conduction band and holes in the valence band. The other two broad peaks at 454

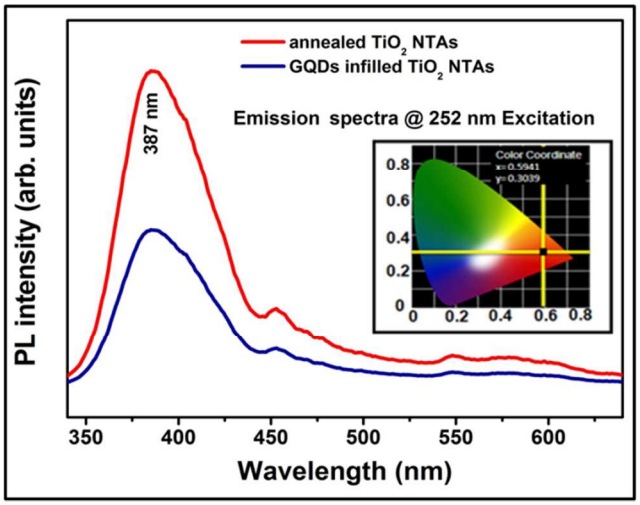

Fig. 8: The PL emission spectra of annealed TiO_2 NTAs and GQDs infilled TiO_2 3D NTAs at 252 nm excitation wavelength; inset exhibits the CIE (chromaticity diagram) color coordinates of annealed TiO_2 3D NTAs, which is obtained from emission spectra of annealed TiO_2 nanotube using chromaticity diagram, x = 0.2243 and y = 0.1808.

nm (~2.73 eV) and 548 nm (~.26 eV) within visible wavelength region corresponds to defects induced photoluminescence either via oxygen defects and impurities and due to surface states induced at annealing temperature. The estimated band gap from

annealed TiO_2 3D NTAs PL spectrum is ~3.2 eV. It is very closely match with the estimated band gap from other spectroscopic technique and also confirms the anatase phase of annealed TiO_2 nanotubes. The PL spectrum of GQDs is shown in Fig. S2c (see supporting information) and inset exhibits strong blue at emission at 320 nm excitation wavelength. A broad peak at 430 nm strong blue emission is observed at 320 nm excitation wavelength.

The optical absorption spectra of annealed TiO_2 3D NTAs and GQDs infilled TiO_2 3D NTAs are shown in Fig. S5 (see supporting information). The samples were dispersed in water and sonicated for 10 min in ultra-sonicater bath. Further, the solution was put in quartz cuvette for UV-visible absorption analysis and reveals that the absorption peak at ~387 nm shown in Fig. S5a. It can be noticed that the intensity of absorption spectra higher in case of GQDs infilled TiO_2 3D NTAs sample. The band gap of annealed sample is estimated using the tauc equation. It is found to be ~3.2 eV, which is expected for TiO_2 anatase phase. The optical absorption spectra of annealed TiO_2 3D NTAs and GQDs infilled TiO_2 3D NTAs samples are also taken in visible light source (mercury lamp) in the range of 400-700 nm, as shown in Fig. S5b. No significant change was observed in presence of visible light source as compared to UV-vis absorption spectra. Thus, the most of photocatalyst phenomenon is driven under UV light. The photocatalyst activity enhancement of the GQD infilled TiO_2 3D NTAs is examined using the reduction of MB in present investigation. The UV-vis absorption spectra of MB solution after being exposed to UV photo-irradiation for different periods of time in the presence of GQD infilled TiO_2 3D NTAs is shown in Fig. 9. The absorption of MB is very strong in the visible range with two well-defined absorption peaks at 612 and 663 nm and the reduced form is colorless. After the illumination of UV light, electrons are excited from the TiO_2 valence band to the conduction band. The photo-generated electrons may then be exploited for reduction of MB. As oxygen is an effective electron scavenger and it is enhanced by introducing GQDs into the TiO_2 nanotubes. It is important to notice that the reaction media is protected with an inert atmosphere of nitrogen. The absorption features diminish rather quickly upon UV photo-irradiation, suggesting the effective photocatalytic activity of GQD infilled TiO_2 in the reduction of MB due to additional surface provide by GQD as well as additional UV absorbed through GQDs surface. The variation of the intensity of the absorption peak at 665 nm with UV exposure time is presented in inset of Fig. 9. It is clear that the absorption peak decreases with respect to time. Thus, the introduction of GQDs into TiO_2 3D NTAs could expand the light absorption range for the broad visible light.

The photocatalytic kinetics activities of the GQDs infilled TiO_2 NTAs were evaluated by photocatalytic degradation of MB in water under UV irradiation light and compared with photocatalytic activity of pristine methylene blue, commercial TiO_2 (purchase from Sigma Aldrich, 99.99 purity, size ~50 nm),

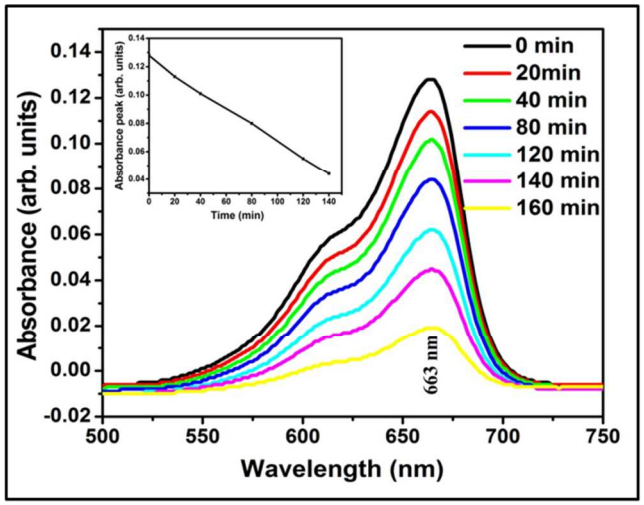

Fig. 9: (a) The UV-vis absorption spectra of MB solution (25 µM in water) after being exposed to UV photo-irradiation for different periods of time in the presence of GQD infilled TiO_2 3D NTAs and inset shows the spectrum of variation of intensity of the absorption peak at 663 nm with UV exposure time for GQD infilled TiO_2 3D NTAs.

as-synthesized TiO_2 nanotubes and annealed TiO_2 nanotubes, as shown in Fig. 10a. It can be seen that the additional surface area and optical property of GQDs and crystallinity of annealed TiO_2 have a strong influence on the photocatalytic activities. The C/C_0 ratio of GQDs infilled TiO_2 nanotubes, annealed TiO_2 nanotubes, as synthesized TiO_2 nanotubes, commercial TiO_2 nanostructures and MB are 0.009, 0.12, 0.39, 0.52 and 0.70, respectively after 180 min irradiation time. In the absence of GQDs, electrons are excited from the valence band (VB) to the conduction band (CB) of TiO_2 and then holes are creating in the valence band. Most of these charges recombine and only a small fraction participates in photocatalytic reactions which decrease the photo-efficiency. Further, after filling the GQDs in TiO_2 NTAs, the degradation rate has faster than the other samples under the same irradiation time and it is exhibited the superior photocatalytic activity for the degradation of MB. About ~99.8% of MB is decomposed for the GQDs infilled TiO_2 annealed samples in 180 min. It may arise from the narrow band gap, reduced charge carriers recombination rate, stabilization and fast electron transport through the GQDs.

Besides its high activity, the stability of the GQDs infilled TiO_2 NTAs sample was also investigated. We examined the stability of GQDs infilled TiO_2 NTAs by repeating the photocatalytic degradation of MB for 10 cycle and calculated data are given in Fig. 10b. It can be seen that the GQDs infilled TiO_2 NTAs sustained a high and stable degradation efficiency of 95.5% after the 10^{th} recycle. The excellent cycling stability is consistent with the nearly unchanged absorption in the visible region. This high cycling stability and reusability of GQDs infilled TiO_2 nanotubes arrays is ascribed to a promising candidate for photocatalytic application. After stability test, we again examined the micro structural morphology of GQDs infilled TiO_2 nanotubes arrays by TEM microscopy, which is shown in Fig. S6 (see supporting information). TEM image exhibits the GQDs remains in TiO_2 nanotube and doesn't

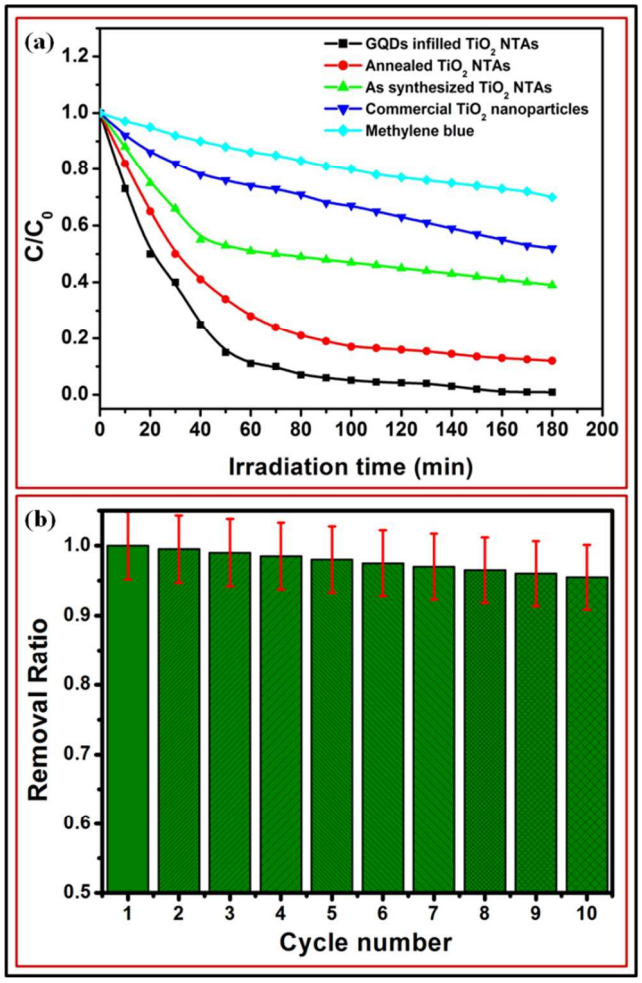

Fig. 10: (a) Comparative studies on photocatalytic activity versus irradiation time of pristine methylene blue, commercial TiO_2 (size ~50nm), as synthesized TiO_2 nanotubes, annealed TiO_2 nanotubes and GQD infilled TiO_2 NTAs and (b) cycle stability data of GQD infilled TiO_2 NTAs.

effect on GQDs after 10th cyclibility test. The surface roughness of TiO_2 nanotube slightly increases.

The schematic illustration of methylene blue photo-degradation process for GQDs infilled TiO_2 nanotube arrays hybrid structure under UV light irradiation is shown in scheme 1. Upon light irradiation, TiO_2 yields electron-holes and electrons are scavenged by oxygen and GQDs to generate "OH^{-1}" radicals and "O^{2-} or H^{+}" intermediate species by reacting with absorbed H_2O molecules for the photodecomposition of MB. Thus, the photo-generated charges are separated efficiently and transferred from TiO_2 conduction band to GQD for radical generation. The strong π-π stacking interaction between MB molecules and large aromatic domains of GQDs creates a high affinity, good electric conductivity and adsorptivity of MB. Moreover, the large specific surface area of GQDs is also increased the adsorption of the MB molecules. Therefore, in the photo degradation of MB, GQDs play an important role to enhance the photocatalytic activity over the pristine TiO_2 NTAs.

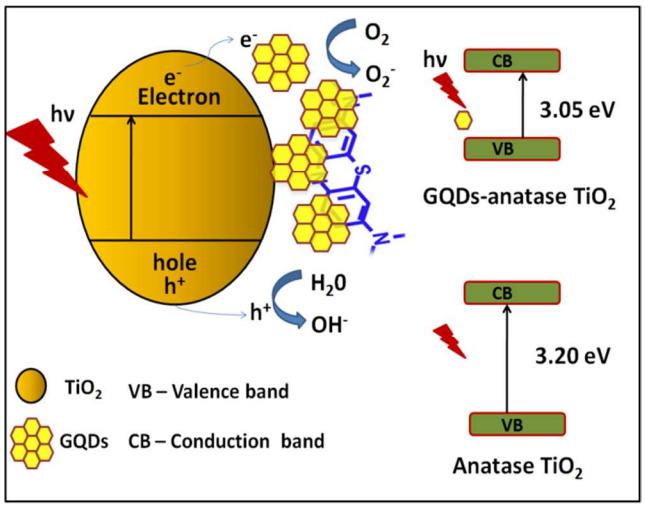

Scheme 1: The schematic illustration of methylene blue photo-degradation process for GQD infilled TiO_2 nanotube arrays hybrid structure under UV light (λ~365 nm) irradiation.

4. Conclusions

A facile method has been demonstrated for the fabrication of GQDs (~8-12 nm) infilled TiO_2 NTAs (~110 nm in diameter) by impregnation of GQDs into TiO_2 nanotubes 3D arrays. The TiO_2 crystallographic structure has remained almost identical for all the composites, and TiO_2 anatase phase is confirmed from both XRD and Raman spectroscopy. Microscopy and spectroscopic studies have revealed that the incorporation of GQDs into the TiO_2 NTAs and the optimal assembly and interfacial coupling between the GQDs and TiO_2 nanotubes, respectively. The activity of GQDs infilled TiO_2 NTAs hybrid structure has expanded the light absorption and enhanced the photocatalytic decomposition of MB molecules in aqueous solution under UV light irradiation. This might be attributed due to the large surface area of GDQs and narrow band gap of TiO_2 in the composite, which would allow greater adsorption of visible light, efficient electron transfer from TiO_2 to GQDs, prolonged recombination rate of charge carriers and oxidation of adsorbed molecules. Thus, it is scalable and cost-effective approach for the fabrication of GQDs infilled TiO_2 NTAs as an efficient multifunctional photocatalyst for the degradation of hazardous compounds in waste water.

Notes and references

[a] *CSIR - National Physical Laboratory, Dr K S Krishnan Road, New Delhi, 110012, India*
[b] *Department of Physics, University of Rajasthan, Jaipur, 302055, India*

** Corresponding author. Tel.: +91-11-45609385, Fx: +91-11-45609310*
E-mail address: bipinbhu@yahoo.com

† Electronic Supplementary Information (ESI) available: [details of any supplementary information available should be included here]. See DOI: 10.1039/b000000x/

‡ Footnotes should appear here. These might include comments relevant to but not central to the matter under discussion, limited experimental and spectral data, and crystallographic data.

Acknowledgments

The authors wish to thank Prof. R. C. Budhani, Director, N.P.L., New Delhi for his keen interest in the work. The authors gratefully acknowledged University Grant Commission (UGC) and Council of Scientific and Industrial Research (CSIR), Govt. of India for financial assistance to carry out this work.

References:

1 A. Fujishima and K. Honda, *Nature*, 1972, **238**, 37-38.
2 J. Xing, W. Fang, H. Zhao and H. Yang, *Chem Asian J*., 2012, **7**, 642-657.
3 N. Wu and M. Lee, *Int. J. Hydrogen Energy*, 2004, **29**, 1601-1605.
4 M. L. Curri, R. Comparelli, P. D. Cozzoli, G. Mascolo and A. Agostiano, *Mater. Sci. Eng., C*, 2003, **23**, 285-289.
5 X. Kang and S. Chen, *J. Mater. Sci.*, 2010, **45**, 2696-2702.
6 J. Zhang, Q. Xu, Z. Feng, M. Li and C. Li, *Angew. Chem. Int. Ed.*, 2008, **47**, 1766-1769.
7 M. J. Uddin, M. M. Alam, M. A. Islam, S. R. Snigda, S. Das, M. M. Rahman, M. N. Uddin. C. A. Morris, R. D. Gonzalez, U. Diebold, T. J. Dickens and O. I. Okoli, *Int. Nano Lett.*, 2013, **3**, 16-26.
8 M. Ni, K. H. Leung, D. Y. C. Leung and K. Sumathy, *Renewable Sustainable Energy Rev.*, 2007, **11**, 401-425.
9 X. Chen and S. S. Mao, *Chem. Rev.,* 2007, **107**, 2891-2895.
10 G. Liu, L. Wang, H. G. Yang, H. M. Cheng and G. Q. Lu, *J. Mater. Chem.,* 2010, **20**, 831-843.
11 M. A. Fox and M. T. Dulay, *Chem. Rev.,* 1993, **93**, 341-357.
12 T. Wu, G. Liu, J. Zhao, H. Hidaka and N. Serpone, *J. Phys. Chem. B,* 1999, **103**, 4862-4867.
13 T. Kako, N. Umezawa, K. Xie and J. Ye, *J. Mater. Sci.,* 2013, **48**, 108-114.
14 J. Macak, M. Zlamal, J. Krysa and P. Schmuki, *Small,* 2007, **3**, 300-304.
15 P. Roy, S. Berger and P. Schmuki, *Angew. Chem. Int. Ed.,* 2011, **50**, 2904-2939.
16 Y. Chen, Y. Tang, S. Luo, C. Liu and Y. Li, *J. Alloys Compd.,* 2013, **578**, 242-248.
17 C. H. Kim, B. H. Kim and K. S. Yang, *Carbon,* 2012, **50**, 2472-2481.
18 M. Nolan, *Chem. Commun.,* 2011, **47**, 8617-8619.
19 Y. Yu, J. Ren and M. Meng, *Int. J. Hydrogen Energy,* 2013, **38**, 12266-12272.
20 P. Song, X. Zhang, M. Sun, X. Cui and Y. Lin, *Nanoscale,* 2012, **4**, 1800-1804.
21 S. Zhu, J. Zhang, X. Liu, B. Li, X. Wang, S. Tang, Q. Meng, Y. Li, C. Shi, R. Hu and B. Yang, *RSC Adv.,* 2012, **2**, 2717-2720.
22 S. Zhuo, M. Shao and S. T. Lee, *ACS nano,* 2012, **6**, 1059-1064.
23 J. Shen, Y. Zhu, X. Yang and C. Li, *Chem. Commun.,* 2012, **48**, 3686-3699.
24 D. Pan, C. Xi, Z. Li, L. Wang, Z. Chen, B. Luc and M. Wu, *J. Mater. Chem.* A, 2013, **1**, 3551-3555.
25 J. Peng, W. Gao, B. K. Gupta, Z. Liu, R. Romero-Aburto, L. Ge, L. Song, L. B. Alemany, X. Zhan, G. Gao, S. Antony Vithayathil, B. A. Kaipparettu, A. A. Marti, T. Hayashi, J. J. Zhu and P. M. Ajayan, *Nano Lett.,* 2012, **12**, 844-849.
26 G. Kedawat, S. Srivastava, V. K. Jain, Pawan, V. Kataria, Y. Agrawal, B. K. Gupta and Y. K. Vijay, *ACS Appl. Mater. Interfaces*, 2013, **5**, 4872-4877.
27 T. Ohsaka, F. Izumi and Y. Fujiki, *J. Raman Spectrosc.,* 1978, **7**, 321-324.